Enhancement of Proton-Boron Nuclear Reactions by Utilizing a Meshed Catcher Target

A.D. Liu,[1] Z.Y. Liu,[1] K. Li,[1] Y.L. Yao,[1] C.T. Zhou,[2] S.P. Zhu,[3] X.T. He,[1,2,3] and B. Qiao[1,4,*]

[1] *Center for Applied Physics and Technology, HEDPS, and SKLNPT, School of Physics, Peking University, Beijing 100871, China*

[2] *Shenzhen Key Laboratory of Ultraintense Laser and Advanced Material Technology, Center for Advanced Material Diagnostic Technology, and College of Engineering Physics, Shenzhen Technology University, Shenzhen 518118, China*

[3] *Institute of Applied Physics and Computational Mathematics, Beijing 100094, China*

[4] *Frontiers Science Center for Nano-optoelectronic, Peking University, Beijing 100094, China*

(Received 29 January 2023; revised 11 July 2023; accepted 30 August 2023; published 22 September 2023)

The proton-boron (pB) reaction has attracted extensive interest for confinement fusion since it produces energetic α particles without neutrons. Based on the pitcher-catcher geometry, a scheme to achieve a high-yielding pB nuclear reaction is proposed, where a meshed catcher target is used. The hot electrons generated by the interaction between laser and pitcher target induce a sheath field in the meshes that accelerates protons in the catcher target to drive a nuclear reaction. Not only is the number of protons increased because the action area of the sheath field becomes larger, but also the energy of protons is well controlled to meet the optimal value by adjusting the size of the mesh based on laser intensity. Two-dimensional particle-in-cell simulations show that our scheme has a 6-times improvement in the yield of nuclear reaction compared with the traditional solid catcher target. With a further increase of laser intensity, the gain of nuclear reaction yield also increases. Our approach provides an idea for the research of laser-driven pB nuclear reaction studies and compact α sources.

DOI: 10.1103/PhysRevApplied.20.034053

I. INTRODUCTION

Aneutronic fusion avoids a lot of energy loss and radiation hazards caused by neutrons in the process of nuclear fusion [1,2]. As one of the candidates to realize aneutronic fusion, the proton-boron (pB) nuclear reaction has attracted the attention of a large number of researchers in recent years. The α particles produced by the pB nuclear reaction have multiple application prospects as secondary sources, such as in cancer therapy [3,4], material irradiation [5], and research on inertial confinement fusion [6]. Therefore it is necessary to achieve a higher yield of the pB nuclear reaction. However, the cross section of this reaction reaches its peak value of about 1.2 barn when the proton energy is 675 keV [7], meaning that the realization of sufficient pB reaction yield under thermal equilibrium conditions requires extremely high temperature and density, which is difficult to achieve under current experimental conditions [8–10].

Thanks to the rapid development of intense lasers [11–13], a laser-driven pB reaction under nonequilibrium conditions has become one of the most effective means to study pB reactions nowadays [14–23]. The most common scheme is the pitcher-catcher geometry [17,18,20], in which a high-intensity laser interacts with a pitcher target to accelerate the protons through the target-normal-sheath-acceleration (TNSA) mechanism [24–29], and then the protons encounter secondary boron solid or plasma (catcher) to induce nuclear reactions. As is well known, the nuclear reaction yield is proportional to the number of protons and the cross section, which depends on the energy of incident protons [7]. Therefore, it is of great importance to both increase the proton number and control the energy in a suitable range. With a higher-intensity laser, it is easier for us to obtain protons with energies of about tens of MeV through the TNSA mechanism. However, when the energy of incident protons is greater than about 5 MeV, the cross section decreases rapidly. Therefore, using the traditional TNSA mechanism to accelerate proton beams for pB reaction in the pitcher-catcher scheme is inefficient, especially for a picosecond (ps) laser with high intensity and long pulse.

Based on the pitcher-catcher geometry, we propose a scheme to enhance the pB nuclear reaction where a meshed catcher target is used. Hot electrons generated by the interaction between laser and pitcher target spread into the meshed target and induce a microsheath field in the meshes; then a large number of protons in the catcher target are accelerated to drive the pB nuclear reaction.

*Correspondence author: bqiao@pku.edu.cn

The meshed target greatly increases the action area of the sheath field to enlarge the number of protons, and controls the proton energy to allow optimization of the nuclear reaction cross section by adjusting the size of meshes based on the laser intensity. Two-dimensional (2D) particle-in-cell (PIC) simulations show that compared with a solid target, the meshed target can bring about a 6-times enhancement in the yield of the pB nuclear reaction, which is also positively correlated with the laser intensity. Our approach provides an idea for the study of laser-driven pB reactions and α sources.

II. THEORETICAL ANALYSIS

The pitcher-catcher scheme with meshed catcher target is shown in Fig. 1(a), which takes advantage of the net charge brought by hot electrons from the pitcher to induce a microsheath field and accelerate protons further. As the protons from the pollution layers are pulled out, the net charge inside the mesh is neutralized gradually, and the electrostatic field gets weakened, then finally disappears. So it can be considered that the electrostatic potential energy brought about by hot electrons in the mesh is converted into the kinetic energy of the protons. To estimate the electrostatic field and the proton temperature theoretically, we solve the Gauss theorem with the mesh setup, and then the expression of the electrostatic field in the mesh can be obtained as

$$\vec{E} = -\frac{e}{2\epsilon_0} n_e \vec{r}, \tag{1}$$

where r is the distance to the center of the mesh and n_e is the electron density. Protons move towards the center of the mesh under the action of electric field, so $E_p = e\int_0^{d/2} \vec{E}\cdot\vec{dr} = (e^2/16\epsilon_0)n_e d^2$. Considering that the net charge is gradually neutralized by protons during the acceleration process, assuming that the net charge density in the mesh decreases linearly with the acceleration process, $T_p = \langle E_p \rangle = (e^2/32\epsilon_0)d^2 n_0$, where n_0 represents the initial density of hot electrons. So, the proton temperature is proportional to the hot electron density and the square of the mesh size. For interaction between intense laser and

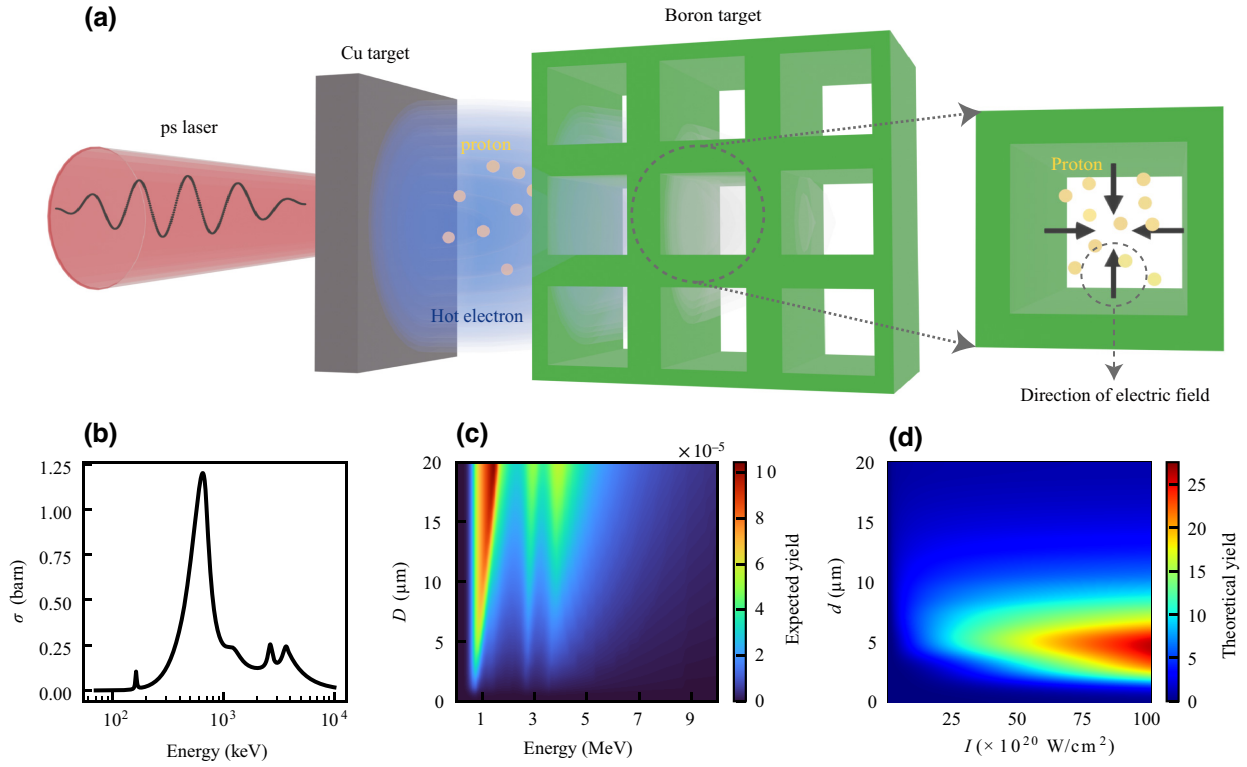

FIG. 1. (a) Setup of the proposed scheme for enhancing the pB reaction by utilizing a meshed catcher target. The blue cloud represents hot electrons that are produced through interaction between a laser and a Cu target. The green meshed boron target is designed as catcher. There are water pollution layers on the inner surface of the meshes that provide protons (yellow spheres). Black arrows represent the direction of the electric field induced by the hot electrons in the mesh. (b) pB cross section versus the energy of protons in the laboratory frame, based on the analytic approximation of Nevins and Swain [8]. (c) Expected nuclear reaction yield of one proton with different energy incident into boron targets with different thickness D. (d) Theoretical prediction of the relationship between nuclear reaction yield, mesh size d, and laser intensity for our scheme, based on $D = 16$ μm. The theoretical yield is normalized by the yield of $d = 10$ μm, $I = 10^{20}$ W/cm^2 cases.

formed plasma, the generated hot electrons follow a pondermotive energy spectrum with a slope temperature $T_h = m_e c^2[(1 + I\lambda_{\mu m}^2/1.37 \times 10^{18})^{1/2} - 1]$ [30]. Assuming that the absorptivity of the laser f is constant for the convenience of theoretical discussion, which is appropriate when the laser intensity is above $I = 1 \times 10^{20}$ W/cm^2 [31,32], it can be estimated that $n_e \propto fI/T_h c$, where c is the speed of light [33]. Combining the two equations, we can get $n_e \propto \sqrt{I}$. Finally, we obtain the relationship between the proton temperature, the mesh size, and the laser intensity: $T_p \propto \sqrt{I}d^2$.

To control variables for direct comparison, the average density of different meshed targets should remain constant. When the meshes become smaller, the internal surface area of the meshes get bigger, which means the sheath field has a larger action area. So it is reasonable to estimate that the number of protons accelerated to induce the nuclear reaction is inversely proportional to the size of meshes. Meanwhile, the higher the density of hot electrons in the meshes, the more protons are required to neutralize the net charge. Therefore, when the mesh size remains the same, the number of protons pulled out in the meshed target should be proportional to the density of hot electrons. In general, $N_p \propto n_e/d$. Based on the above analysis, the spectrum of accelerated protons can be presented as

$$\frac{dN_p}{dE} = \frac{C_1}{d^3} \exp\left(-E/C_2\sqrt{I}d^2\right). \tag{2}$$

C_1 and C_2 are constants, which are related to specific laser and target parameters.

The calculation formula of pB nuclear reaction yield in pitcher-catcher geometry is as follows [16]:

$$N_\alpha = 3n_B \int \left(\int_{E^* - E_{\text{change}}}^{E^*} \frac{\sigma(E)}{\epsilon(E)}\, dE \right) \frac{dN_p}{dE^*} dE^*, \tag{3}$$

where $E_{\text{change}} = \int_0^D \epsilon(E(x))dx$, $\epsilon(E)$ represents the stopping power of protons in cold boron targets, $\sigma(E)$ represents the cross section of the pB nuclear reaction, and D is the thickness of the boron target. Different from a thermonuclear reaction, the influence of stopping power should be considered in this geometry, which is the deceleration effect caused by the collision of solid cold boron targets with protons. The nuclear reaction rate $\sigma v dt$ can therefore be rewritten as $\sigma v dt = \sigma dx = (\sigma/dE/dx)dE = (\sigma/\epsilon)dE$. Figure 1(c) shows the expected nuclear reaction yield of one proton with different energy incident into a boron target with different thickness. Due to the stopping power, the proton energy decreases dramatically, and then the nuclear reaction cross section decreases. Therefore, although the peak of the pB reaction is located at 675 keV, the maximum of the expected reaction yield does not always correspond to the peak, but changes with the thickness of the target. It can be noticed from Fig. 1(c) that when the proton energy is greater than 1 MeV and the thickness is larger than 10 μm, the expected yield of the nuclear reaction is close to the maximum value. There is a trend shown in Fig. 1(c) that the expected yield will increase as the proton energy and target thickness continue to increase, but considering the accelerated proton spectrum, the number of protons decreases exponentially with the increase of energy, so it is most appropriate to use 1-MeV protons to drive the nuclear reaction.

Substituting Eq. (2) into the above equation and setting the thickness D as 16 μm as the range of 1-MeV protons in the boron target is about 12.58 μm [34], the relationship between the nuclear reaction yield and laser intensity and mesh size can be obtained, as shown in Fig. 1(d). It can be found that with a fixed laser intensity, the nuclear reaction yield increases first, and then decreases with the increase of the mesh size, which means that there is an optimal value. This is because the increase of the mesh size will increase the proton temperature, making the number of protons that are at about 1 MeV increase. However, as the mesh size continues to increase, the total number of protons accelerated decreases since the total area of the sheath field decreases. With an increase of laser intensity, the yield of the nuclear reaction increases under the optimum mesh size. The theoretical calculation shows that with the laser intensity increasing from 1×10^{20} to 1×10^{22} W/cm^2, the yield also increases by 30 times, that is, the yield of the nuclear reaction increases with an increase of laser intensity in our scheme.

All in all, by adjusting the size of the mesh, the acceleration process of protons in the target can be well controlled for the nuclear reaction, which is an advantage that cannot be realized in a traditional pitcher-catcher scheme based on TNSA.

III. SIMULATION RESULTS

As presented explicitly in Eq. (3), the nuclear reaction rate is related to the cross section and the stopping power in the pitcher-catcher geometry. Due to the stopping power, protons will lose energy when moving in the catcher target, while the cross section is also changed along with the proton energy dynamically. Therefore, simulations with ion stopping power and nuclear reaction are necessary for analyzing the whole process in detail. In our 2D EPOCH code [35], nuclear reaction calculation module and stopping power of ions from SRIM table are all implemented, which can iterate self-consistently during the evolution of the laser-plasma system [36–38]. By the way, in the simulation only the main channel of the pB reaction, $p + {}^{11}\text{B} \longrightarrow \alpha_1 + {}^{8}\text{Be}^* + 5.65\ \text{MeV} \longrightarrow \alpha_1 + \alpha_{11} + \alpha_{12}$, has been included for less complexity, which mostly contributes to the nuclear reaction cross section [39].

The simulation box size is 170×12 μm^2 with a spatial resolution of 10 nm in both the longitudinal (x) and transversal (y) directions. The boundary condition is simple-outflow and periodic, respectively, in x and y directions. A laser pulse with $I = 1 \times 10^{20}$ W/cm^2, $\lambda = 1.053$ μm, and p polarization propagates in the $+x$ direction, which is a plane wave and Gaussian with duration $\tau = 0.5$ ps in temporal profile. A copper target with thickness of 10 μm and $100n_c$ is set as the pitcher located at 0 μm. Preplasma with scale length $\lambda = 3$ μm is also included in front of the pitcher target. The macroparticles in each cell for electrons and Cu ions are 80 and 40. For the catcher target, a boron target is placed from $x = 30$ μm to $x = 126$ μm for both the solid target case and meshed target case whose density is also $n_e = 100n_c$. The macroparticles in each cell for electrons and boron ions are 48 and 24. The meshed target consists of periodically arranged square meshes with period size $d = 10$ and 12 μm, so the thickness of the boron filled in the x direction D is about 16 μm, corresponding to the range of 1-MeV protons discussed above. There is a pollution layer with thickness of 300 nm and $n_e = 100n_c$ attached on the surface of each of Cu target and boron target, which provides the protons for the pB reaction. The macroparticles in each cell for electrons, protons, and oxygen ions are 100, 80, and 24, respectively. We use a third-order particle shape in order to avoid artificially softening the edges of meshes while avoiding numerical self-heating. The initial plasma temperatures are both set to 0. The numerical convergence is confirmed by comparing the physical quantities of interest with simulations with different macroparticle numbers per cell and with the two codes, EPOCH and WarpX [40].

As mentioned above, hot electrons produced by the interaction of ps laser and pitcher target induce a microsheath field, which plays a key role in enhancing the nuclear reaction. As shown in Fig. 2(a), hot electrons are generated from the pitcher target and expand into the meshed target, then bring about a net charge to each mesh. According to Gauss's theorem, an electric field will be generated in the mesh, which is directed towards the center of the mesh, as shown in Figs. 2(b) and 2(c) corresponding to E_x and E_y, respectively. Since the hot electron density does not change much within the size range of the mesh, we assume that the hot electrons are uniformly distributed, which can be given by the simulation results in Fig. 2(a) as $n_e = 3 \times 10^{-2} n_c$. Figures 2(d) and 2(e) show a comparison between the simulation results of E_x and E_y in the mesh and the theoretical results of Eq. (1), respectively, which are in good agreement. It is worth noting that there is a difference between the simulation results and the formula at the edge of the mesh, as the symmetry required by the Gaussian theorem is disrupted. Considering that we are concerned about the work done by the electric field on the protons in the mesh, the difference in electric field at the edge has a negligible impact on our theoretical analysis. Simulations

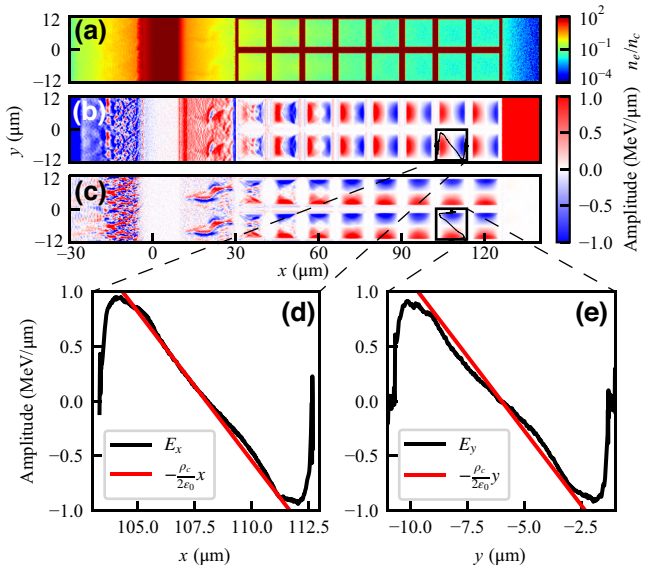

FIG. 2. 2D snapshots of (a) electron densities n_e, (b) electric fields E_x, and (c) electric fields E_y at $t = 1$ ps. Black solid line in (b),(c) represents the electric field distribution along this axis. The black boxes correspond to the distribution of (d) E_x and (e) E_y along the axis in the mesh.

show that the electric field will exist until enough protons are accelerated into the meshes to neutralize the hot electron charge.

With this physical process, a large number of protons whose energies are around 1 MeV to drive the nuclear reaction can be obtained. Figure 3(a) shows the proton energy spectrum of meshed target case and solid target case. The red curve shows the spectrum of protons accelerated in the meshes at $t = 2.76$ ps, when the electrostatic field inside the meshed target disappears. It is easy to see that the corresponding cross sections of the protons accelerated in the meshed target are all above 0.1 barn. For the solid target case, the reaction cross section corresponding to the energy of protons entering the catcher is very small. Meanwhile, the meshes increases the action area of the sheath field, which means that the number of protons accelerated in the meshed target is far more than that entering the solid target leading to more low-energy protons to better drive the pB nuclear reaction. The above two factors lead to the enhancement of the nuclear reaction of the meshed target, which is shown in Fig. 3(b) as the temporal evolution of the pB reaction yield and the production rate for solid target and meshed target. Due to the limitation of computing resources, we only simulate the physical process for 6 ps. In the process we simulate, the number of reaction events in the meshed target case is 3 times that of the solid target case. In the inset of Fig. 3(b), the production rate of the solid target case decreases by 2 orders of magnitude at $t = 6$ ps. For the meshed target case, the production rate is starting to decrease. Therefore, it is

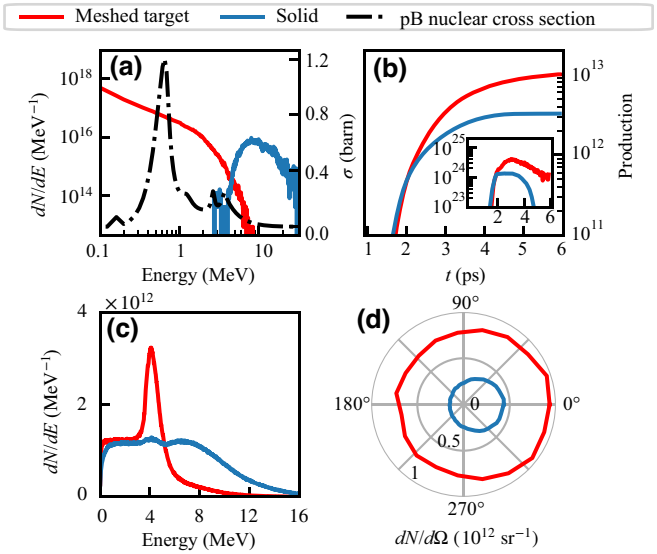

FIG. 3. (a) The spectra of protons accelerated in meshes (red) and protons entering the solid catcher from pitcher (blue). Black dash-dotted curve represents pB fusion cross section as a function of proton energy in the laboratory [8]. (b) Temporal evolution of the yield of the pB nuclear reaction, the inset showing the temporal evolution of the production rate. (c) The α-particle energy spectrum of the two cases. For the convenience of comparison, the value of the blue curve (solid target case) is increased 4 times. (d) The α-particle angular distribution for both cases.

reasonable to believe that the yield of the meshed target case can be 6 times higher than that of the solid target case when the whole process is completed. We substitute the fitting of proton energy spectrum of the two cases into Eq. (3) and verify the above conclusion through numerical calculation. Figures 3(c) and 3(d) show the α-particle energy spectra and angular distributions of the two cases. Compared with the solid target case, the energy spectrum of the α particles of the meshed target case is peaked at about 4 MeV, while the solid target case production has a large energy broadening. This is because the proton energy involved in the reaction in the meshed target is low, and the α-particle energy mainly comes from the energy released by the nuclear reaction, which is about 4 MeV [41]. In the case of solid target, the protons involved in the nuclear reaction are far more energetic, so they will transfer more energy to α particles, which brings about the broadening of the energy spectrum shown as the blue curve in Fig. 3(c). What is more, the protons accelerated by the planar target through TNSA have strong forward directional characteristic, which also leads to the forward directional characteristic of the α particles of the solid target case. The protons accelerated in the meshed target tend to be isotropic, as do the α particles generated. Although the directivity of the products from the meshed target is not as good as that from the solid target case, due to the huge increase in the number of reaction events, the number of forward α particles is still larger than that of the solid target, as shown in Fig. 3(d). Combined with the energy spectrum with good monoenergetic characteristics, the meshed target may have more application scenarios as a secondary α-particle source. From the application perspective, it is necessary to discuss whether α particles can be ejected from boron targets. In the meshed target, α particles need to pass through an average of 8 μm of boron to get out of the target, while α particles in solid targets need to pass through tens of micrometers of boron to exit. According to the calculation results of SRIM, a range of 8 μm corresponds to 3-MeV α particles, which is less than the main α-particle energy generated by the meshed target, which is above 4 MeV. Therefore, compared with solid targets, a significant fraction of α particles generated in the meshed target can escape and are more conducive to practical applications.

The influence of different mesh size and laser intensity on the nuclear reaction should be discussed further for optimization. Figure 4(a) shows energy spectra of the protons inside the meshes at the moment the electric field in the meshes disappears for different cases, and the total yield for each cases is presented in Fig. 4(b). When the mesh size of the meshed target is small, for example, 4 and 5 μm, a large number of accelerated protons cannot reach the first peak of expected yield around 1 MeV, which leads to an enhancement of reaction events only about 1–2 times compared with the case of the solid target. When the meshes become bigger, for example, 8, 10, and 16 μm, more protons are accelerated to 1–5 MeV, which results in a higher yield of the nuclear reaction. The number of protons accelerated is counted and the temperature of protons in different meshed targets is also fitted, which is shown in Fig. 4(c). As the mesh size increases, the number of protons participating in the nuclear reaction decreases because of the smaller action area for the sheath field, which is consistent with our previous theoretical analysis. Also, it can be seen in Fig. 4(c) that the proton temperature is close to being proportional to the square of mesh size, which is also consistent with our theoretical estimation. In our theoretical prediction, based on the laser and target parameters we use, the optimal mesh size is around 8–12 μm. Therefore, for a fixed laser intensity, there is an optimal mesh size. Figure 4(d) shows the proton energy spectrum for protons accelerated in different meshed targets under different laser intensity, which is set based on the best condition in Fig. 1(d). It can be seen that with a linear increase of $\sqrt{I}$, with a corresponding decrease in the size of the mesh, the final proton temperature is almost unchanged, but the number of protons increases obviously, which will inevitably lead to an increase in nuclear reaction yields, which is shown in Fig. 4(e). Simulation shows that when the laser intensity is enhanced to $I = 1.6 \times 10^{21}$ W/cm^2, the yield of reaction using a meshed target with a mesh of 4 μm has an order-of-magnitude increase compared

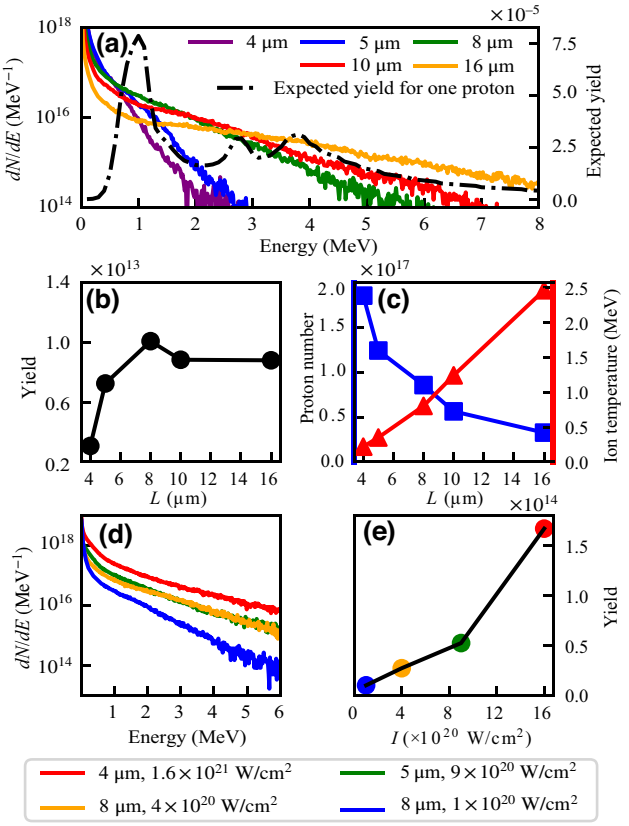

FIG. 4. (a) Spectra of the protons at the moment of electric field disappearance in different meshed targets, symbolized by different colors. Black dash-dotted line represents the expected yield for one proton for different energy. (b) The yields of nuclear reaction for different meshed target cases. (c) Number of protons that are accelerated and proton temperature from meshed targets with different parameters. (d) Spectra of the protons of optimal meshed targets for different laser intensity. (e) The yields of nuclear reaction for the different cases in (d).

with that for $I = 1 \times 10^{20}$ W/cm^2 and mesh of 8 μm. It is obvious that with this laser intensity, the higher-energy protons brought about by traditional TNSA with a solid target will not increase the number of nuclear reaction events in pitcher-catcher mode, but only lead to α particles generated with higher energy. It is worth mentioning that from the perspective of fusion energy applications, this scheme is insufficient. Taking the case of $I = 1 \times 10^{20}$ W/cm^2, $d = 8$ μm as an example, the total laser energy is about 20 J, while the energy released by the pB reaction is about 1×10^{-4} J. The conversion rate from laser energy to fusion energy is about 5×10^{-4}%.

IV. SUMMARY AND DISCUSSION

In summary, a scheme for laser-driven pB reaction enhancement based on pitcher-catcher geometry by utilizing a meshed catcher target is explored. First of all, the meshes increase the interaction area of the accelerating protons by the microsheath field, which greatly increases the number of protons. Secondly, compared with the traditional TNSA mechanism that accelerates protons to tens of MeV, the microsheath field accelerates protons to the MeV level, which greatly increases the cross section of the pB nuclear reaction. 2D PIC simulations show that the microsheath field induced by hot electrons in the meshes results in a 6-times improvement in the yield of the pB nuclear reaction. Since the energy of the protons is relatively low, the distribution in space of α particles produced tends to be isotropic and the energy of α particles is mainly around 4 MeV.

Furthermore, we explore the control of proton acceleration through adjusting the laser intensity and the parameters of the meshed target, which could be also predicted by the theoretical analysis. The size of the meshes affects the number of protons accelerated in the catcher target and also their temperature. The larger the mesh, the fewer the protons, and the higher the temperature. Simulations confirm that there is an optimal mesh size for the determined laser parameters, which provides a clear theoretical basis for the experimental realization of this scheme. With increasing laser intensity, the size of meshes should be reduced to increase the number of protons while keeping the proton energy still near 1 MeV, further increasing the yield of nuclear reactions. This kind of dynamic control of the interaction process to realize optimization is absolutely not available for the traditional pitcher-catcher scheme. As the laser intensity increases by 1 order of magnitude, the nuclear reaction yield also increases by 1 order of magnitude under the optimal conditions of the meshed target. With the development of laser technology, the intensity and duration of lasers continue to increase, and our approach can provide more possibilities for further application of and research into pB reactions.

ACKNOWLEDGMENTS

This work is supported by the National Key R&D Program of China, Grants No. 2022YFA1603200 and No. 2022YFA1603201; National Natural Science Foundation of China, Grants No. 12135001, No. 11921006, and No. 11825502; Strategic Priority Research Program of CAS, Grant No. XDA25050900. BQ acknowledges support from the National Natural Science Funds for Distinguished Young Scholar, Grant No. 11825502. The simulations are carried out on the Tianhe-2 supercomputer at the National Supercomputer Center in Guangzhou.

[1] G. L. Kulcinski and J. F. Santarius, Advanced fuels under debate, Nature **396**, 724 (1998).
[2] N. Rostoker, M. W. Binderbauer, and H. J. Monkhorst, Colliding beam fusion reactor, Science **278**, 1419 (1997).

[3] D.-K. Yoon, J.-Y. Jung, and T. S. Suh, Application of proton boron fusion reaction to radiation therapy: A Monte Carlo simulation study, Appl. Phys. Lett. **105**, 223507 (2014).
[4] G. Cirrone, L. Manti, D. Margarone, G. Petringa, L. Giuffrida, A. Minopoli, A. Picciotto, G. Russo, F. Cammarata, and P. Pisciotta, *et al.*, First experimental proof of proton boron capture therapy (pbct) to enhance proton therapy effectiveness, Sci. Rep. **8**, 1 (2018).
[5] G. Petringa, G. Cirrone, C. Caliri, G. Cuttone, L. Giuffrida, G. Larosa, R. Manna, L. Manti, V. Marchese, and C. Marchetta, *et al.*, Study of gamma-ray emission by proton beam interaction with injected boron atoms for future medical imaging applications, J. Instrum. **12**, C03049 (2017).
[6] number M. Temporal, B. Canaud, W. Cayzac, R. Ramis, and R. L. Singleton, Effects of alpha stopping power modelling on the ignition threshold in a directly-driven inertial confinement fusion capsule, Eur. Phys. J. D **71**, 1 (2017).
[7] S. Stave, M. Ahmed, R. France III, S. Henshaw, B. Müller, B. Perdue, R. Prior, M. Spraker, and H. Weller, Understanding the b11 (p, α) α α reaction at the 0.675 meV resonance, Phys. Lett. B **696**, 26 (2011).
[8] W. Nevins and R. Swain, The thermonuclear fusion rate coefficient for p-11b reactions, Nucl. Fusion **40**, 865 (2000).
[9] D. C. Moreau, Potentiality of the proton-boron fuel for controlled thermonuclear fusion, Nucl. Fusion **17**, 13 (1977).
[10] J. Martinez-Val, S. Eliezer, M. Piera, and G. Velarde, Fusion burning waves in proton-boron-11 plasmas, Phys. Lett. A **216**, 142 (1996).
[11] P. Maine, D. Strickland, P. Bado, M. Pessot, and G. Mourou, Generation of ultrahigh peak power pulses by chirped pulse amplification, IEEE J. Quantum Electron. **24**, 398 (1988).
[12] T. Boehly, R. Craxton, T. Hinterman, J. Kelly, T. Kessler, S. Kumpan, S. Letzring, R. McCrory, S. Morse, and W. Seka, *et al.*, The upgrade to the omega laser system, Rev. Sci. Instrum. **66**, 508 (1995).
[13] G. H. Miller, E. I. Moses, and C. R. Wuest, The national ignition facility, Opt. Eng. **43**, 2841 (2004).
[14] A. Picciotto, D. Margarone, A. Velyhan, P. Bellutti, J. Krasa, A. Szydlowsky, G. Bertuccio, Y. Shi, A. Mangione, and J. e. Prokupek, *et al.*, Boron-proton nuclear-fusion enhancement induced in boron-doped silicon targets by low-contrast pulsed laser, Phys. Rev. X **4**, 031030 (2014).
[15] D. Margarone, A. Picciotto, A. Velyhan, J. Krasa, M. Kucharik, A. Mangione, A. Szydlowsky, A. Malinowska, G. Bertuccio, and Y. Shi, *et al.*, Advanced scheme for high-yield laser driven nuclear reactions, Plasma Phys. Controlled Fusion **57**, 014030 (2014).
[16] L. Giuffrida, F. Belloni, D. Margarone, G. Petringa, G. Milluzzo, V. Scuderi, A. Velyhan, M. Rosinski, A. Picciotto, and M. Kucharik, *et al.*, High-current stream of energetic α particles from laser-driven proton-boron fusion, Phys. Rev. E **101**, 013204 (2020).
[17] D. Margarone, A. Morace, J. Bonvalet, Y. Abe, V. Kantarelou, D. Raffestin, L. Giuffrida, P. Nicolai, M. Tosca, and A. Picciotto, *et al.*, Generation of α-particle beams with a multi-kJ, peta-watt class laser system, Front. Phys. 343 (2020).
[18] J. Bonvalet, P. Nicolaï, D. Raffestin, E. D'humieres, D. Batani, V. Tikhonchuk, V. Kantarelou, L. Giuffrida, M. Tosca, and G. Korn, *et al.*, Energetic α-particle sources produced through proton-boron reactions by high-energy high-intensity laser beams, Phys. Rev. E **103**, 053202 (2021).
[19] V. Belyaev, A. Matafonov, V. Vinogradov, V. Krainov, V. Lisitsa, A. Roussetski, G. Ignatyev, and V. Andrianov, Observation of neutronless fusion reactions in picosecond laser plasmas, Phys. Rev. E **72**, 026406 (2005).
[20] C. Labaune, C. Baccou, S. Depierreux, C. Goyon, G. Loisel, V. Yahia, and J. Rafelski, Fusion reactions initiated by laser-accelerated particle beams in a laser-produced plasma, Nat. Commun. **4**, 1 (2013).
[21] C. Labaune, C. Baccou, V. Yahia, C. Neuville, and J. Rafelski, Laser-initiated primary and secondary nuclear reactions in boron-nitride, Sci. Rep. **6**, 1 (2016).
[22] D. Margarone, J. Bonvalet, L. Giuffrida, A. Morace, V. Kantarelou, M. Tosca, D. Raffestin, P. Nicolai, A. Picciotto, and Y. Abe, *et al.*, In-target proton–boron nuclear fusion using a pW-class laser, Appl. Sci. **12**, 1444 (2022).
[23] C. Baccou, S. Depierreux, V. Yahia, C. Neuville, C. Goyon, R. De Angelis, F. Consoli, J. Ducret, G. Boutoux, and J. Rafelski, *et al.*, New scheme to produce aneutronic fusion reactions by laser-accelerated ions, Laser Particle Beams **33**, 117 (2015).
[24] A. Macchi, M. Borghesi, and M. Passoni, Ion acceleration by superintense laser-plasma interaction, Rev. Mod. Phys. **85**, 751 (2013).
[25] R. Snavely, M. Key, S. Hatchett, T. Cowan, M. Roth, T. Phillips, M. Stoyer, E. Henry, T. Sangster, and M. Singh, *et al.*, Intense High-Energy Proton Beams from Petawatt-Laser Irradiation of Solids, Phys. Rev. Lett. **85**, 2945 (2000).
[26] B. Qiao, M. Foord, M. Wei, R. Stephens, M. Key, H. McLean, P. Patel, and F. Beg, Dynamics of high-energy proton beam acceleration and focusing from hemisphere-cone targets by high-intensity lasers, Phys. Rev. E **87**, 013108 (2013).
[27] T. Bartal, M. E. Foord, C. Bellei, M. H. Key, K. A. Flippo, S. A. Gaillard, D. T. Offermann, P. K. Patel, L. C. Jarrott, and D. P. Higginson, *et al.*, Focusing of short-pulse high-intensity laser-accelerated proton beams, Nat. Phys. **8**, 139 (2012).
[28] P. Mora, Plasma Expansion into a Vacuum, Phys. Rev. Lett. **90**, 185002 (2003).
[29] X. F. Shen, A. Pukhov, and B. Qiao, Monoenergetic high-energy ion source via femtosecond laser interacting with a microtape, Phys. Rev. X **11**, 041002 (2021).
[30] S. C. Wilks, W. L. Kruer, M. Tabak, and A. B. Langdon, Absorption of Ultra-Intense Laser Pulses, Phys. Rev. Lett. **69**, 1383 (1992).
[31] M. G. Haines, M. S. Wei, F. N. Beg, and R. B. Stephens, Hot-Electron Temperature and Laser-Light Absorption in Fast Ignition, Phys. Rev. Lett. **102**, 045008 (2009).
[32] Y. Ping, R. Shepherd, B. F. Lasinski, M. Tabak, H. Chen, H. K. Chung, K. B. Fournier, S. B. Hansen, A. Kemp, D. A. Liedahl, K. Widmann, S. C. Wilks, W. Rozmus, and M. Sherlock, Absorption of Short Laser Pulses on Solid

Targets in the Ultrarelativistic Regime, Phys. Rev. Lett. **100**, 085004 (2008).

[33] J. Fuchs, P. Antici, E. d'Humières, E. Lefebvre, M. Borghesi, E. Brambrink, C. Cecchetti, M. Kaluza, V. Malka, and M. Manclossi, *et al.*, Laser-driven proton scaling laws and new paths towards energy increase, Nat. Phys. **2**, 48 (2006).

[34] J. F. Ziegler and J. P. Biersack, Srim-2013, http://www.srim.org (2013).

[35] T. Arber, K. Bennett, C. Brady, A. Lawrence-Douglas, M. Ramsay, N. Sircombe, P. Gillies, R. Evans, H. Schmitz, and A. Bell, *et al.*, Contemporary particle-in-cell approach to laser-plasma modelling, Plasma Phys. Controlled Fusion **57**, 113001 (2015).

[36] Z. Liu, K. Li, Y. Yao, Z. Lei, C. Zhou, S. Zhu, X. He, and B. Qiao, Enhancement of nuclear reactions via the kinetic Weibel instability in plasmas, Plasma Phys. Controlled Fusion **63**, 125030 (2021).

[37] D. P. Higginson, A. Link, and A. Schmidt, A pairwise nuclear fusion algorithm for weighted particle-in-cell plasma simulations, J. Comput. Phys. **388**, 439 (2019).

[38] T. A. Mehlhorn, A finite material temperature model for ion energy deposition in ion-driven inertial confinement fusion targets, J. Appl. Phys. **52**, 6522 (1981).

[39] H. Becker, C. Rolfs, and H. Trautvetter, Low-energy cross sections for11b (p, 3α), Z. für Phys. A At. Nucl. **327**, 341 (1987).

[40] L. Fedeli, A. Huebl, F. Boillod-Cerneux, T. Clark, K. Gott, C. Hillairet, S. Jaure, A. Leblanc, R. Lehe, A. Myers, C. Piechurski, M. Sato, N. Zaim, W. Zhang, J.-L. Vay, and H. Vincenti, in *SC22: International Conference for High Performance Computing, Networking, Storage and Analysis* (2022), p. 1.

[41] V. Dmitriev, α-particle spectrum in the reaction p+ 11b$\rightarrow$ α+ 8be*$\rightarrow$ 3α, Phys. At. Nucl. **72**, 1165 (2009).